Systems pharmacology of the amyloid cascade : unfolding oligomer modulation in Alzheimer's disease

Maanen, E.M.T. van

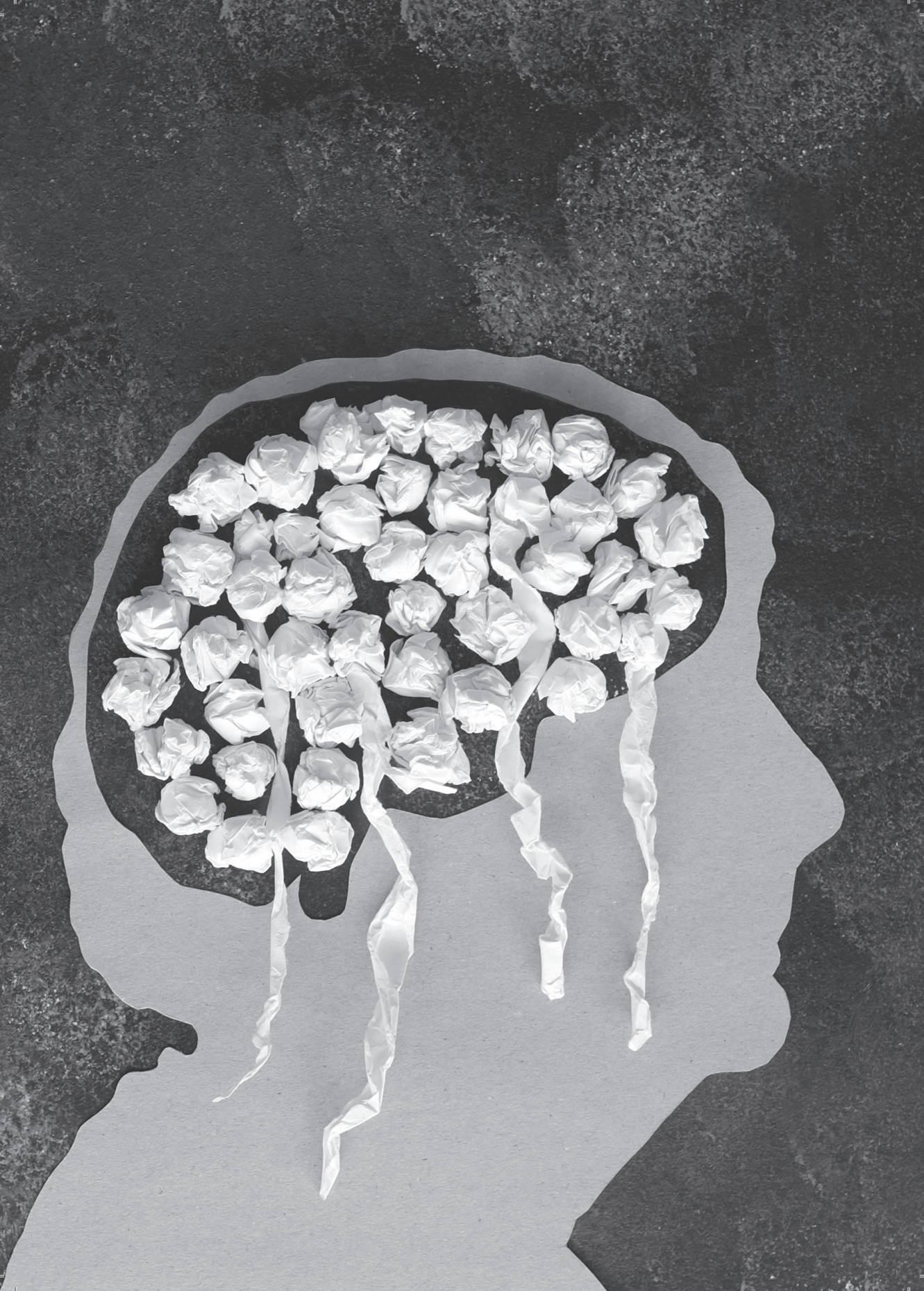

Chapter 7

A single systems pharmacology approach to unravel Aβ oligomer modulation upon administration of multiple APP cleavage inhibitors

E.M.T. van Maanen, T.J. van Steeg, J. Kalinina, M.S. Michener,
M.J. Savage, M.E. Kennedy, J.A. Stone, M. Danhof

Abstract

Accumulation of toxic soluble Aβ oligomers (Aβ_{O}) is the primary event driving the pathological changes in Alzheimer's Disease (AD). Inhibition of β-amyloid precursor protein (APP) cleavage enzymes has been proposed as an approach to reduce Aβ_{O} concentrations. Due to the complexity of the underlying biochemical network, the effects of these interventions on Aβ_{O} are difficult to predict.

The aim of this investigation was to develop a single systems pharmacology model to predict the change in Aβ_{O} following administration of inhibitors of multiple APP cleavage enzymes (i.e. β-secretase (BACE1) and γ-secretase (GS) inhibition). A novel systems pharmacology model, the β-γ-O-APP model, which is an extension of a previously proposed β-O-APP model, was successfully applied to describe the pharmacokinetics and the time course of the changes in APP metabolite (sAPPβ, sAPPα, Aβ42, Aβ40, Aβ38) and Aβ_{O} concentrations.

A differential effect of BACE1 versus GS inhibition on the APP metabolite profiles was observed, which was reflected in the ratio Aβ42:Aβ40:Aβ38. The analysis shows that this may be explained by stepwise successive cleavage of C99 by GS, wherein part of Aβ38 is converted from Aβ42. Both BACE1 and GS inhibition resulted in similar maximum reduction of the Aβ_{O} and monomeric Aβ. The β-γ-O-APP model suggests that GS inhibition may enhance the non-amyloidogenic processing of APP via homeostatic feedback exerted by C99. Understanding the mechanisms that underlie the APP processing pathway through the APP systems pharmacology model aids the optimization of therapeutic intervention to reduce Aβ_{O} burden.

Introduction

The amyloid cascade hypothesis for Alzheimer's Disease (AD) posits that the deposition of the amyloid peptides (Aβ) in the brain is a central event in the pathophysiology. Aβ s are elevated early in the disease, before clinical symptoms manifest and this leads to a series of pathophysiological changes [1]. The most toxic species of Aβ are soluble Aβ oligomers (Aβ_O), which are believed to be the initial drivers of neurodegeneration [2,3]

Aβ is the final product of proteolytic cleavage of the transmembrane β-amyloid precursor protein (APP) and the precursor of Aβ_O. In the amyloidogenic pathway, Aβ is produced by sequential cleavage of APP by β-secretase 1 (BACE1) and γ-secretase (GS) [4]. Cleavage by BACE1 creates the soluble β-amyloid precursor protein (sAPPβ) and C99, a C-terminal fragment which remains membrane bound. Aβ is derived from the GS cleavage of C99, generating Aβ peptides of various amino acid chain lengths, of which the most common are 38, 40 or 42 amino acids long (Aβ38, Aβ40, or Aβ42, respectively) [5]. An alternative pathway is driven by α-secretase cleavage, which generates the non-amyloidogenic soluble sAPPα and the C-terminal membrane-bound 83-amino acid fragment C83. This occurs within the Aβ sequence, and thus precludes Aβ generation [6].

Aβ peptide accumulates in stages into amyloid plaques. The Aβ peptides first form Aβ_O, which are soluble disordered clusters. Then, protofibrils are formed, which are prefibrillar insoluble high molecular weight Aβ_O (50-1500 kDa) consisting of spherical, annular, and curvilinear assemblies [7,8,9]. Next, chains of agglomerates called fibrils are generated, followed by an interwoven mass of fibrils called β-sheets and in the final stage plaques are developed [10].

Targeting Aβ_O may prove to be an effective treatment for AD by halting their accumulation and preventing their neurotoxic effect. One of the main therapeutic strategies for AD aims at Aβ reduction through inhibition of Aβ production. Due to the complexity of the underlying biochemical network, the effects of these interventions on the individual moieties of the APP processing pathways and Aβ_O are difficult to predict.

Systems pharmacology abstracts our understanding of biochemical/pathological pathways into mathematical constructs, in combination with the application of pharmacokinetic (PK) and pharmacodynamic (PD) principles. In this approach, the drug effect is considered to be the result of the interactions of the drug and the biological system.

Recently, we have proposed a systems pharmacology model of the APP processing pathway characterizing APP metabolite (sAPPα, sAPPα, Aβ40, Aβ42, Aβ38) and Aβ_O responses to BACE1 inhibition, the so called β-O-APP model [11]. In that inves-

tigation Aβ oligomerization was identified to display second order kinetics and Aβ42 was found to be the major contributor to the Aβ_{O} pool. This model was based on an analysis of the data of the effect of a BACE1 inhibitor from a 4-way crossover study in cisterna-magna-ported rhesus monkeys on the effects of a BACE1 (MBi-5) and a GS (MK-0752) inhibitor on the biomarker concentrations in CSF. In the current investigation, we have included the GS inhibitor response data from the same study and investigated differences in biomarker responses between BACE1 and GS inhibition.

In an earlier analysis with the β-γ-APP model, both BACE1 and GS inhibition were predicted to lower Aβ_{O} levels, which was at that point derived from monomeric Aβ dynamics[12]. The prediction suggested a lower oligomerization rate of Aβ42 after GS and BACE1 inhibition. Now, the effect of BACE1 and GS inhibition on the time course of the changes in Aβ_{O} measurements is determined and can be compared. Also, to our knowledge for the first time, sAPPβ and sAPPα levels following GS inhibition have been measured.

The objectives of this investigation were: (1) to extend a systems pharmacology model of the APP processing pathway, describing the effects of both BACE1 and GS inhibitors on its individual attributes and its interrelationships; (2) to elucidate the relationship between the Aβ_{O} and monomeric Aβ further, which is imperative to improve the prediction of therapeutic effects on Aβ; (3) to understand the difference in Aβ dynamics following BACE1 *versus* GS inhibition.

Materials and Methods

Animals

In this study, six male rhesus monkeys, weighing between 8.6 kg and 11.8 kg (mean, 9.7 kg), age at 9 years to 13 years (mean, 11 years) at time of the study were included. They were individually housed and captive-bred in a closed colony. The rhesus monkeys are chronically implanted with catheters in the cisterna magna, as described by Gilberto et al.[13]. This facilitated repeated sampling of CSF and plasma in conscious rhesus monkeys. All animal studies were reviewed and approved by the MSD Institutional Animal Care and Use Committee. The NIH Guide to the care and use of Laboratory Animals and the Animal Welfare act were followed in the conduct of the animal studies (Institute of Laboratory Animal Resources, National Research Council, 1996).

Drug administration and sampling

In a four-way full crossover study, a single oral dose of MBi-5 at 30 and 125 mg/kg, MK-0752 at 240 mg/kg (5 mL/kg) or vehicle (0.4% methylcellulose) was administered. Plasma and CSF drug concentrations were collected at 0 (predose) and 3, 5, 7, 9, 13, 14.5, 16, 19, 22, 25, 28, 31, 49, 55, 58, 73 and 96 h postdose, resulting in 18 plasma and CSF PK samples for each rhesus monkey per treatment group. 2 mL of blood and 1 mL of CSF were collected at each time point. The concentration of MBi-5 and MK-0752 in the plasma and CSF samples was determined using LC-MS/MS. The concentrations of sAPPα, sAPPβ, Aβ40, Aβ42, Aβ38 and Aβ_{O} were determined from CSF samples, collected at the same time points as PK samples, by established and validated ELISA-based assays (Meso Scale Diagnostics "sAPPα/sAPPβ Kit" (Catalog No. K15120E) and "Human (6E10) Abeta Triplex Assay" (Catalog No. K15148E)), giving 18 measurements of each biomarker for each monkey per treatment. To determine Aβ_{O} concentrations, a two-site ELISA assay was used, that was previously described by Savage et al. [14].

PK-PD analysis

A non-linear mixed effects modelling approach was used to analyze the PK and PD data. This approach takes structural (fixed) effects and both intra- and interindividual variability into account. Typical values of structural model parameters (population parameters, which define the average value for a parameter in a population) (θ), the variance and covariance of the interindividual variability (ω^2) and the variance of the residual error (σ^2) are estimated. The population approach described individual profiles relative to the overall population trend.

The β-γ-O-APP model was implemented in the software package NONMEM (version 7.2.0 [15]). The models were compiled using Compaq Visual Fortran (version 6.6, Compaq Computer Corporation, Houston, Texas, USA) and executed on a PC equipped with an an Intel QuadCore (Intel® Core^{TM} i7 CPU860, 2.80 GHz, 3.24 GB RAM). Data management and model assessment was done using the statistical software package S-PLUS for Windows (version 8.0 Professional, Insightful Corp., Seattle, USA). Based on the analysis of their obtained minimum value of the objective function (defined as minus twice the log-likelihood), the precision of parameter estimates, and visual inspection of goodness-of-fit plots the best models were selected. A more detailed description of the modelling procedure was described in van Maanen et al. [16].

The performance of the β-γ-O-APP model was evaluated with a visual predictive check (VPC), in which the median and the 90% inter-quantile range of the data simulated

with the final parameter estimates were plotted together with the observations. A validated result would have close resemblance of median observed and predicted line with 90% of the observations that fall within the 90% prediction interval.

Berkeley Madonna™ version 8.3.18 (Macey and Oster, University of California, Berkeley) was used for simulations to illustrate the characteristics of the β-γ-O-APP model.

Model description

The APP systems pharmacology model was developed by sequential analysis of PK and PD data following administration of MBi-5 and MK-0752. The PK model of MBi-5 was based on simultaneous analysis of plasma and CSF PK data and has been described elsewhere by van Maanen et al. [16]. The PK model for MK-0752 was reported previously [17,12]. The PK models adequately described the plasma and CSF concentration time profiles of MBi-5 and MK-0752, respectively, thus the models could serve as input for PD model analysis.

The biomarker response profiles of MBi-5 and MK-0752 measured in CSF were adequately described by the β-γ-O-APP model containing compartments for eight moieties: APP, sAPPβ, sAPPα, C99, Aβ40, Aβ42, Aβ38 and Aβ_{O} (Fig. 7.1). APP production was assumed to be constant and described by a zero order input rate Rin_{APP}. The production of the APP metabolites was assumed to be first order, i.e. dependent on its precursor concentration. The interaction between APP and its metabolites (sAPPβ, sAPPα, C99, Aβ40, Aβ42 and Aβ38) and Aβ_{O} is described by Eq. 7.1 - Eq. 7.8:

$$\frac{d}{dt}APP = Rin_{APP} - \left(Rin\beta \times EFFB + Rin\alpha \times \left(\frac{C99}{C99_{base}} \right)^{FP} \right) \times APP \tag{7.1}$$

$$\frac{d}{dt}sAPP\alpha = Rin\alpha \times \left(\frac{C99}{C99_{base}} \right)^{FP} \times APP - Rout_a \times sAPP\alpha \tag{7.2}$$

$$\frac{d}{dt}sAPP\beta = Rin\beta \times EFFB \times APP - Rout_b * sAPP\beta \tag{7.3}$$

$$\begin{aligned}\frac{d}{dt}C99 =& Rin\beta \times EFFB \times APP \\ &- (Kin_{40} + Kin_{42} + Kin_{38}) * EFFG * C99 - Kout_{99} * C99\end{aligned} \tag{7.4}$$

$$\frac{d}{dt}A\beta_{40} = Kin_{40} \times EFFG \times C99 - Kout \times A\beta_{40} \tag{7.5}$$

$$\begin{aligned}\frac{d}{dt}A\beta_{42} =& Kin_{42} \times EFFG \times C99 - Kout_{42} \times A\beta_{42} \\ &- Kin_{382} \times EFFG \times A\beta_{42} - Kpl \times (A\beta_{42})^{ALPH} \\ &+ Krev \times A\beta_O / \left(\frac{MW_{A\beta 42}}{1000} \times Factor_{oligo}\right)\end{aligned} \tag{7.6}$$

$$\begin{aligned}\frac{d}{dt}A\beta_{38} =& Kin_{38} \times EFFG \times C99 + Kin_{382} \times EFFG \times A\beta_{42} \\ &- Kout * A\beta_{38}\end{aligned} \tag{7.7}$$

$$\frac{d}{dt}A\beta_O = Kpl \times (A\beta_{42})^{ALPH} \times \frac{MW_{A\beta 42}}{1000} \times Factor_{oligo} - Krev \times A\beta_O \tag{7.8}$$

The rate of change of APP with respect to time in the presence of the BACE1 inhibitor is expressed by Eq. 7.1, in which the BACE1 cleavage inhibition is incorporated by the factor *EFFB*. The rate of change of C99 with respect to time in the presence of the GS inhibitor is described by Eq. 7.4, in which the GS cleavage inhibition is incorporated by the factor *EFFG*. *EFFB* and *EFFG* are the degrees of inhibition caused by MBi-5 and MK-0752, respectively. Generally, the degree of inhibition is described by a sigmoidal Imax function, as shown in Eq. 7.9.

$$EFF = 1 - \frac{C_{target}^{GAM} * Imax}{C_{target}^{GAM} + IC50^{GAM}} \tag{7.9}$$

Where C_{target} is the target site concentration of MBi-5 or MK-0752, respectively, *IC50* the C_{target} that results in 50% inhibition of BACE1 or GS, *Imax* is the maximum response and *GAM* is the Hill coefficient. C_{target} was derived from the respective PK models as:

$$C_{target} = C_{plasma} * \frac{AUC_{CSF}}{AUC_{plasma}} \tag{7.10}$$

Where AUC_{CSF} and AUC_{plasma} are the areas under the CSF and plasma concentration time curves, respectively. C_{target} is assumed to be at a level between C_{CSF} and C_{plasma}, following the same profile as C_{plasma}.
It is assumed that the system is in steady state (SS) when no treatment is given *(EFFB=1, EFFG=1)*. These steady state conditions were used to derive part of the system parameters. From SS and Eq. 7.1 it follows that the zero order input rate of APP *(Rin_{APP})* is:

$$Rin_{APP} = (Rin_{\alpha} + Rin_{\beta}) * APP_{base} \tag{7.11}$$

Where APP_{base} is the baseline level of APP, assumed to be equal to the sum of the baseline levels of sAPPα and sAPPβ, as all alternate pathways are represented by the terms for α-secretase.

Using SS conditions and Eq. 7.2 the sAPPα formation rate (Rin_{α}), equivalent to the α-secretase cleavage step, can be derived:

$$Rin_{\alpha} = Rout_{a} \times \frac{sAPP\alpha_{base}}{APP_{base}} \tag{7.12}$$

Where sAPPα_{base} is the baseline level of sAPPα.

The sAPPβ and C99 formation rate (Rin_{β}), equivalent to the BACE1 cleavage step, follows from SS conditions and Eq. 7.3:

$$Rin_{\beta} = Rout_{b} \times \frac{sAPP\beta_{base}}{APP_{base}} \tag{7.13}$$

Where $sAPP\beta_{base}$ is the baseline level of sAPPβ.

From Eq. 7.5 and SS, the Aβ degradation rate (*Kout*), is deduced:

$$Kout = Kin_{40} \times \frac{C99_{base}}{A\beta 40_{base}} \tag{7.14}$$

Where $C99_{base}$ is the baseline level of C99.

From Eq. 7.4 and SS the baseline level of C99 can be derived:

$$C99_{base} = \frac{Rout_b \times sAPP\beta_{base} \times A\beta 40_{base}}{Kin_{40} \times (A\beta 40_{base} + A\beta 38_{base} + A\beta 42_{base}) + A\beta 40_{base} \times Kout_{99}} \tag{7.15}$$

Using SS conditions 7.6, 7.7 and 7.15, respectively, the formation rates of Aβ42 (*Kin42*) and Aβ38 (*Kin38*), equivalent to γ-secretase cleavage steps, can be calculated:

$$Kin_{42} = \frac{(Kout + Kin_{382}) \times A\beta 42_{base}}{C99_{base}} \tag{7.16}$$

$$Kin_{38} = \frac{Kout \times A\beta 38_{base} - Kin_{382} \times A\beta 42_{base}}{C99_{base}} \tag{7.17}$$

Where $A\beta 42_{\mathrm{base}}$ and $A\beta 38_{\mathrm{base}}$ are the baseline levels of Aβ42 and Aβ38, receptively.

The exchange between the $A\beta_{\mathrm{O}}$ pool and the Aβ42 compartment is described by Eq. 7.6 and Eq. 7.8, where *ALPH* is the power of the concentration of Aβ42, $Factor_{oligo}$ is the conversion factor on $A\beta_{\mathrm{O}}$ and $MW_{A\beta 42}$ is the molecular weight of Aβ42. *Krev* and *Kpl* are the dissociation rate and higher-order Aβ42 oligomerization rate constant, respectively, which are dependent on the baseline values of Aβ42 and the $A\beta_{\mathrm{O}}$ pool ($A\beta 42_{\mathrm{base}}$ and $A\beta_{\mathrm{O\,base}}$, resp.) according to Eq. 7.18:

$$Krev = \frac{Kpl \times (A\beta_{42base})^{ALPH} \times \frac{MW_{AB42}}{1000} \times Factor_{oligo}}{A\beta_{Obase}} \tag{7.18}$$

The model structure includes six transit compartments (Fig. 7.1), one for each biomarker measured in CSF (sAPPα, sAPPβ, Aβ40, Aβ42, Aβ38, $A\beta_{\mathrm{O}}$), to account for transport from the target site in the brain to CSF. These transit processes are described, in general, by Eq. 7.19:

$$\frac{d}{dt}xAx_{CSF} = Ktr * (xAx - xAx_{CSF}) \tag{7.19}$$

Where *Kt* is the transit rate for the particular particular APP metabolite xAx (*KtAP* for sAPPα and sAPPβ and *KtAB* for Aβ40, Aβ42, Aβ38 and Aβ_{O}).

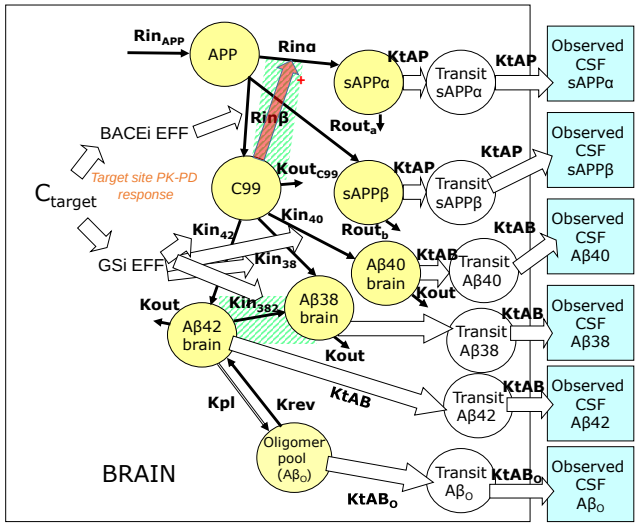

Figure 7.1: Schematic of β-γ-O-APP model.
The model comprised fourteen compartments: Eight biomarker compartments in brain *(yellow circles)* and six transit compartments from brain to CSF *(white circles)*. Six biomarkers were measured in CSF (sAPPα, sAPPβ, Aβ40,Aβ42, Aβ38 and Aβ_{O}), indicated by the blue boxes. The drug effect of the BACE1 inhibitor *(BACEi EFF)* inhibited *Rin*β. The drug effect of the GS inhibitor *(GSi EFF)* inhibited *Kin*$_{40}$, *Kin*$_{40}$, *Kin*$_{38}$ and *Kin*$_{382}$. As driver of biomarker response C_{target} was used, which was derived from the PK models of the BACE1 inhibitor[16] and GS inhibitor[12], respectively. The red arrow indicates the homeostatic feedback on α-secretase through the action of C99. Model extensions compared to the β-O-APP model are indicated with the green shaded area.
APP: Aβ-precursor protein; *A*β: amyloid-β-peptide; C_{target}: drug concentration target site; *Kin*$_{38}$: Aβ38 formation rate from C99; *Kin*$_{382}$: Aβ38 formation rate from Aβ42; *Kin*$_{40}$: Aβ40 formation rate; *Kin*$_{42}$: Aβ42 formation rate; *Kout*: Aβ38, Aβ40 and Aβ42 degradation rate; *Kout*$_{C99}$: C99 degradation rate; *Krev*: Oligomer dissociation rate; *KtAP*: transit rate sAPPα and sAPPβ from brain to CSF; *Kpl*: Oligomerization rate; *KtAB*: transit rate Aβ from brain to CSF; *KtAB*$_O$: transit rate Aβ_{O} from brain to CSF; *RinAPP*: source of APP; *Rin*β: sAPPβ formation rate; *Rin*α: sAPPα formation rate; *Routb*: sAPPβ degradation rate; *Routa*: sAPPα degradation rate.

Results

APP systems pharmacology model

A systems pharmacology model, incorporating the PK of MBi-5 and MK-0752, CSF APP metabolite (Aβ38, Aβ40, Aβ42, sAPPα and sAPPβ) concentrations and Aβ_O measurements was developed to quantify APP metabolite and Aβ_O responses to BACE1 and GS inhibition in monkeys. The model, named the β-γ-O-APP model, is schematically presented in Fig. 7.1. The model included terms to describe the production and elimination of each APP metabolite. The oligomerization of Aβ42 was described by higher order kinetics[11].

The drug effect of MBi-5 was incorporated in the model as blocking sAPPβ and C99 production, equivalent to the BACE1 cleavage step. The drug effect of MK-0752 was implemented as blocking Aβ production, corresponding to the GS cleavage step. Both drug effects where described by an Imax function[12].

Part of Aβ38 is converted from Aβ42

A difference in the ratios of Aβ42, Aβ40 and Aβ38 over total Aβ (Aβ38+Aβ40+Aβ42) following BACE1 versus GS inhibition was found (see Supplemental Material). This was described by extending the β-γ-O-APP model to account for subsequent GS cleavage of part of Aβ42 to Aβ38 (Equation 7.7). This cleavage step is inhibited by the GS inhibitor, but not blocked if BACE1 is inhibited.

MK-0752 exposure increased sAPPα

A slight decrease in sAPPβ and increase of sAPPα concentrations, as well as a change in the ratio sAPPβ:sAPPα was observed in response to GS inhibition (see Supplemental Material). This could be described by implementing a homeostatic feedback loop in the model structure regulated by C99: The increase in C99 relative to baseline C99 after GS inhibition stimulates α-secretase processing of APP (Equation 7.2). Then, as result of substrate competition, BACE1 processing of APP relatively decreases resulting in a slight decline of sAPPβ following GS inhibition. The strength of this homeostatic feedback action was quantified by the feedback parameter *FP*, that was estimated to be 0.438, which was significantly different from zero (when there would be no feedback).

Aβ production inhibition decreased $A\beta_O$

Both BACE1 and GS inhibition reduced the $A\beta_O$ levels, which was adequately described by the APP systems model (Figs. 7.3F, 7.4F and 7.5F, respectively). Note that Aβ monomers were measured in pM and $A\beta_O$ were expressed in pg/mL. For this reason, a conversion factor needed to be included in the model, which was discussed recently [11]. A similar maximum reduction of $A\beta_O$ concentration of 89% was obtained after treatment with 125 mg/kg MBi-5 and 240 mg/kg MK-0752. However, GS inhibition had a more prolonged pharmacological effect on $A\beta_O$ levels compared to BACE1 inhibition.

Model parameters

The analysis of the variability of model parameters due to interanimal variation resulted in a random-effects structure including interanimal variability for the baselines of sAPPβ, sAPPα, Aβ38, Aβ40, Aβ42 and $A\beta_O$, with the same random-effect parameter used for Aβ40 and Aβ42 (Table 7.2). All were included as exponential in nature, which reflects lognormal distributions of the individual parameters.

It was not possible to obtain a successful completion of the Covariance Step in NONMEM using the model including interanimal variability. Furthermore, because of long model minimization times it was not feasible to perform a bootstrap to obtain parameter precision. Therefore, the precision of the model parameters from the model without interanimal variability is reported in Table 7.1, which was adequate.

To take caution against over parameterization of the model, the formation rate constant of Aβ40 Kin_{40} was fixed to the value from the β-O-APP model [11].

When estimated, the Hill coefficients of the concentration response relationships of MBi-5 and MK-0752 were not significantly different from 1. Therefore, the sigmoid-Imax concentration response relationships could be simplified to Imax relationships by fixing the Hill coefficients to 1. For MBi-5, a potency (IC50) of 0.0251 μM (95% CI, 0.02-0.0302) was identified, which was similar to the previously reported IC50 of 0.0256 μM (95% CI, 0.0137–0.0375) from another CMP rhesus study [16], and is also near the *in vitro* inhibition constant (Ki) of 10 nM for MBi-5 inhibition of purified BACE1 and the IC50 of 24 nM for inhibition of Aβ production in intact cells [18]. An IC50 of 0.0468 μM (95% CI, 0.0154–0.0782) was identified for MK-0752 . This value was 10 fold lower than reported earlier for CMP rhesus monkeys [12] and also 10 fold lower than the brain IC50 of MK-0752 in guinea-pigs of 440 nM [19].

Table 7.1: Population parameter estimates including coefficient of variation (CV%)

PARAMETER	DESCRIPTION	VALUE	UNIT	CV%
Structural parameters				
$\text{sAPP}\beta_{\text{base}}$	baseline sAPPβ	382	pM	17
$\text{A}\beta38_{\text{base}}$	baseline Aβ38	411	pM	16
$\text{A}\beta40_{\text{base}}$	baseline Aβ40	1330	pM	10.5
$\text{A}\beta42_{\text{base}}$	baseline Aβ42	107	pM	12.1
$\text{sAPP}\alpha_{\text{base}}$	baseline sAPPα	457	pM	13.3
Kin_{40}[a]	formation rate Aβ40	1.29	h^{-1}	
Kin_{382}	Aβ38 formation rate from Aβ42	0.162	h^{-1}	17.5
Rout_{a}	degradation rate sAPPα	1.11	h^{-1}	12.7
Rout_{b}	degradation rate sAPPβ	1.46	h^{-1}	11.8
Kout_{99}	degradation rate C99	0.496	h^{-1}	34.9
KtAP	transit rate sAPPα and sAPPβ	0.122	h^{-1}	3.09
KtAB[a]	transit rate Aβ	10	h^{-1}	
ImaxB[a]	maximal inhibition (Imax) MBi-5	1		
IC_{50}B	median inhibition concentration MBi-5	0.0251	μM	10.4
GAMB[a]	Hill coefficient MBi-5	1		
ImaxG[a]	maximal inhibition (Imax) MK-0752	1		
IC_{50}G	median inhibition concentration MK-0752	0.0468	μM	34.2
GAMG[a]	Hill coefficient MK-0752	1		
Kpl	oligomerization rate	5.46e-4	$\text{pM}^{-1}\ \text{h}^{-1}$	40.1
$\text{A}\beta_{\text{Obase}}$	baseline $\text{A}\beta_{\text{O}}$	2.03	pg/mL	13.6
ALPH[a]	order oligomerization	2		
FP	feedback parameter	0.496		20.8
Factor_{oligo}	conversion factor on oligomers	0.00994		20.6
Residual error				
${\sigma^2}_{\text{A}\beta40}$ [b]	Residual variability Aβ40	0.157		21.5
${\sigma^2}_{\text{A}\beta42}$ [b]	Residual variability Aβ42	0.146		26.9
${\sigma^2}_{\text{sAPP}\beta}$ [b]	Residual variability sAPPβ	0.269		42.8
${\sigma^2}_{\text{sAPP}\alpha}$ [b]	Residual variability sAPPα	0.175		34.9
${\sigma^2}_{\text{oligo}}$ [b]	Residual variability $\text{A}\beta_{\text{O}}$	1.01		18.2
${\sigma^2}_{\text{A}\beta38}$ [b]	Residual variability Aβ38	0.247		27.1

[a] Fixed.

[b] Residual variability is assumed to follow a normal distribution with mean zero and variance σ^2.

Table 7.2: Population parameter estimates

PARAMETER	DESCRIPTION	VALUE	UNIT
Structural parameters			
$sAPP\beta_{base}$	baseline sAPPβ	349	pM
$A\beta38_{base}$	baseline Aβ38	373	pM
$A\beta40_{base}$	baseline Aβ40	1250	pM
$A\beta42_{base}$	baseline Aβ42	98	pM
$sAPP\alpha_{base}$	baseline sAPPα	423	pM
Kin_{40} [a]	formation rate Aβ40	1.29	h^{-1}
Kin_{382}	Aβ38 formation rate from Aβ42	0.145	h^{-1}
$Rout_a$	degradation rate sAPPα	1.08	h^{-1}
$Rout_b$	degradation rate sAPPβ	1.54	h^{-1}
$Kout_{99}$	degradation rate C99	0.386	h^{-1}
KtAP	transit rate sAPPα and sAPPβ	0.129	h^{-1}
KtAB [a]	transit rate Aβ	10	h^{-1}
ImaxB [a]	maximal inhibition (Imax) MBi-5	1	
$IC_{50}B$	median inhibition concentration MBi-5	0.0255	μM
GAMB [a]	Hill coefficient MBi-5	1	
ImaxG [a]	maximal inhibition (Imax) MK-0752	1	
$IC_{50}G$	median inhibition concentration MK-0752	0.0488	μM
GAMG [a]	Hill coefficient MK-0752	1	
Kpl	oligomerization rate	6.45e-4	$pM^{-1}\ h^{-1}$
$A\beta_{O\,base}$	baseline Aβ_O	1.75	pg/mL
ALPH [a]	order oligomerization	2	
FP	feedback parameter	0.438	
$Factor_{oligo}$	conversion factor on oligomers	0.00667	
Interanimal variability			
ω^2_{BSAPb} [b]	Interanimal variability sAPPβ baseline	0.194	
ω^2_{BSAPa} [b]	Interanimal variability sAPPα baseline	0.105	
$\omega^2_{AB4.}$ [b]	Interanimal variability Aβ40 and Aβ42	0.0681	
ω^2_{AB38} [b]	Interanimal variability Aβ38	0.119	
ω^2_{ABO} [b]	Interanimal variability Aβ_O	0.116	
Residual error			
$\sigma^2_{A\beta40}$ [c]	Residual variability Aβ40	0.117	
$\sigma^2_{A\beta42}$ [c]	Residual variability Aβ42	0.0705	
$\sigma^2_{sAPP\beta}$ [c]	Residual variability sAPPβ	0.109	
$\sigma^2_{sAPP\alpha}$ [c]	Residual variability sAPPα	0.0783	
σ^2_{oligo} [c]	Residual variability Aβ_O	0.785	
$\sigma^2_{A\beta38}$ [c]	Residual variability Aβ38	0.0934	

[a] Fixed.

[b] Interanimal variability is assumed to follow a normal distribution with mean zero and variance ω^2.

[c] Residual variability is assumed to follow a normal distribution with mean zero and variance σ^2.

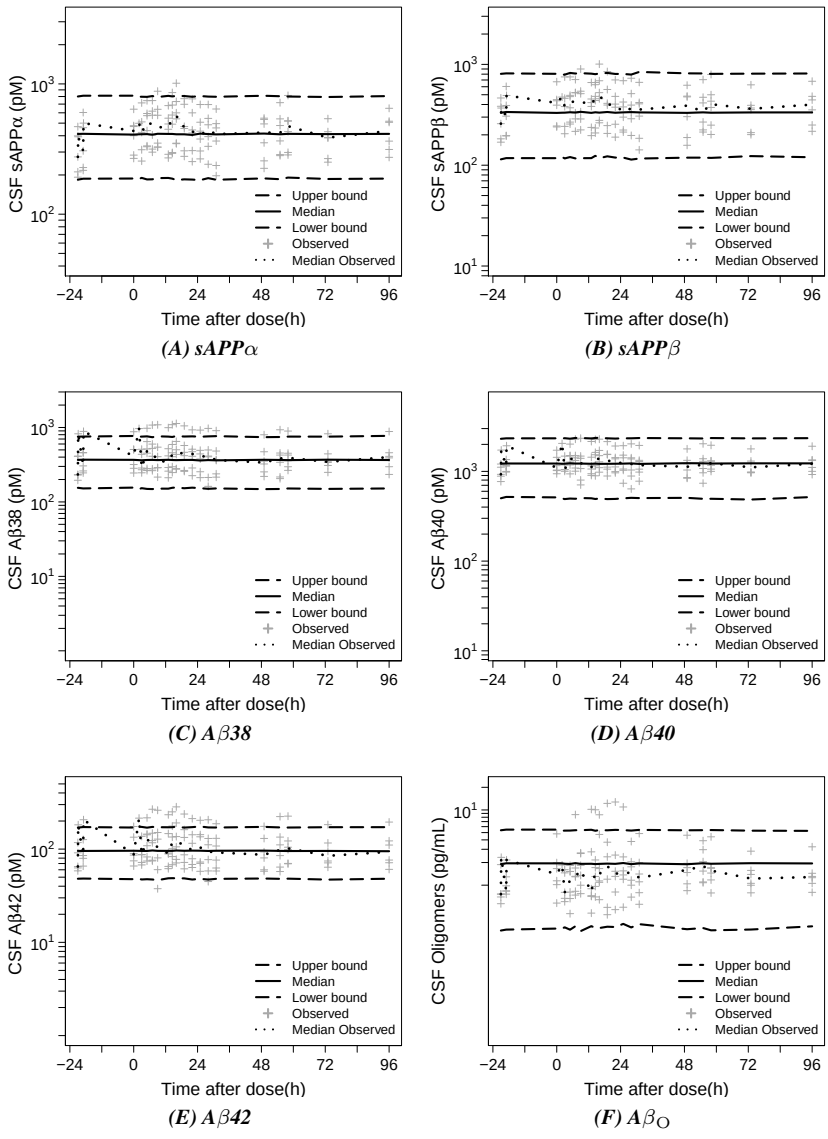

Figure 7.2: Placebo. Visual predictive check of biomarker response* vs. *time profile of placebo in the rhesus with 90% confidence interval. Predictions were performed with extended model ((A), (B), (C), (D), (E), (F)). Observation sample size: n=108 for each APP metabolite from 6 monkeys collected over 4 days.

Plus-symbols represent observed measurements. Dotted blue line corresponds to the median observed profile. Solid lines show the median simulated profiles. The long-dashed lines correspond to the 90% prediction intervals obtained from 1000 individual simulated profiles.

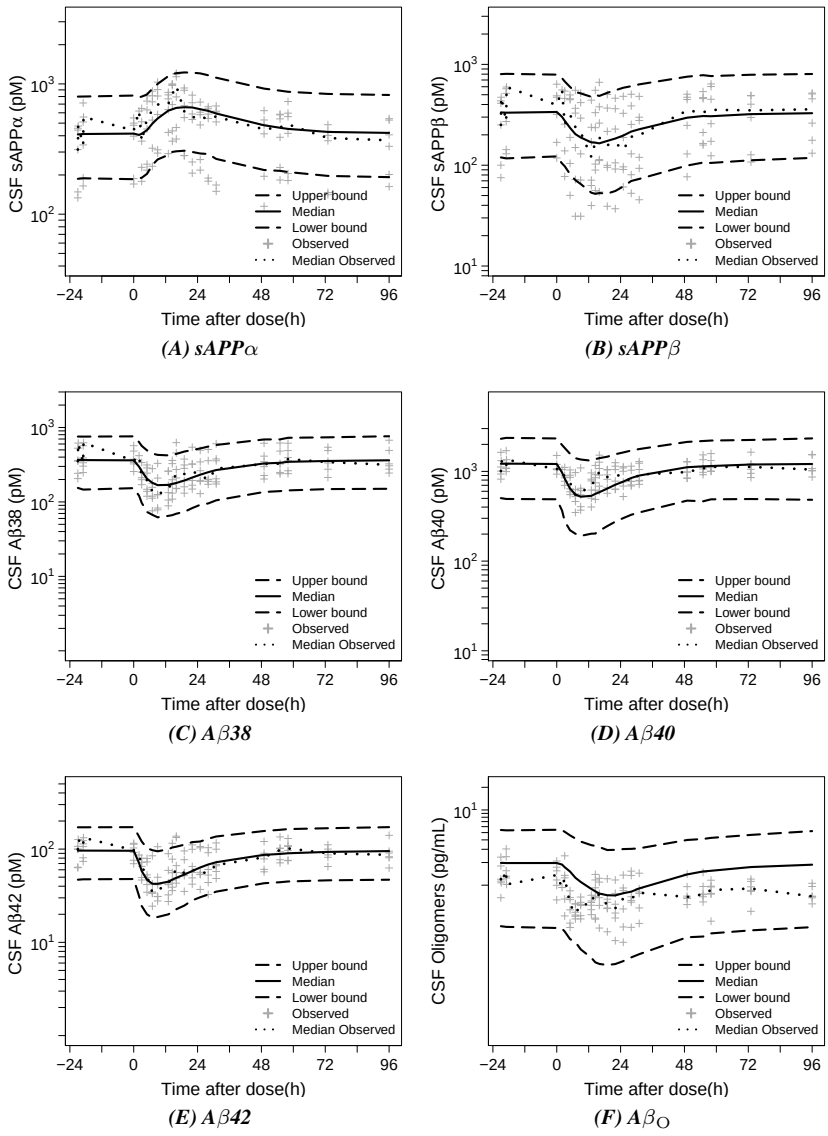

Figure 7.3: Dose 30 mg/kg MBi-5. Visual predictive check of biomarker response* vs. *time profile of MBi-5 in the rhesus with 90% confidence interval. Predictions were performed with model with extended model ((A), (B),(C), (D), (E),(F)). Observation sample size: n=108 for each APP metabolite from 6 monkeys collected over 4 days.

Plus-symbols represent observed measurements. Dotted blue line corresponds to the median observed profile. Solid lines show the median simulated profiles. The long-dashed lines correspond to the 90% prediction intervals obtained from 1000 individual simulated profiles.

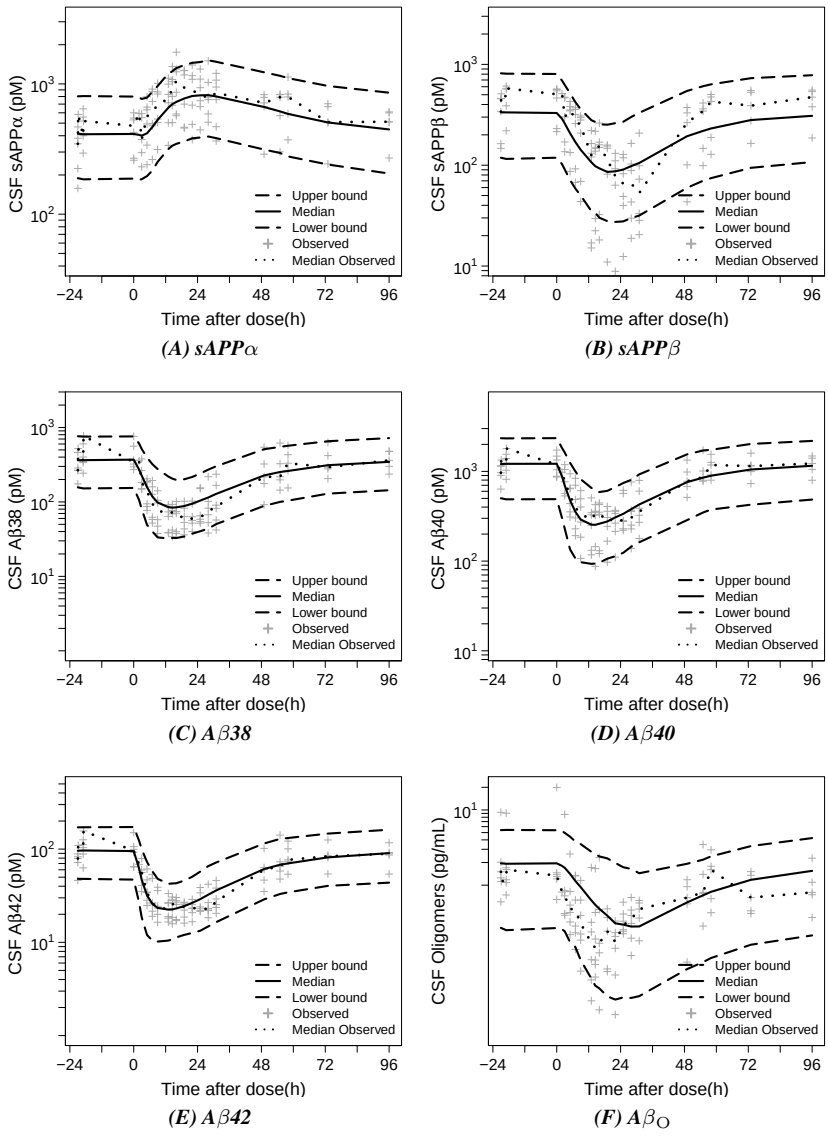

Figure 7.4: Dose 125 mg/kg MBi-5. Visual predictive check of biomarker response* vs. *time profile of MBi-5 in the rhesus with 90% confidence interval. Predictions were performed with extended model ((A), (B),(C), (D), (E),(F)). Observation sample size: n=108 for each APP metabolite from 6 monkeys collected over 4 days.

Plus-symbols represent observed measurements. Dotted blue line corresponds to the median observed profile. Solid lines show the median simulated profiles. The long-dashed lines correspond to the 90% prediction intervals obtained from 1000 individual simulated profiles.

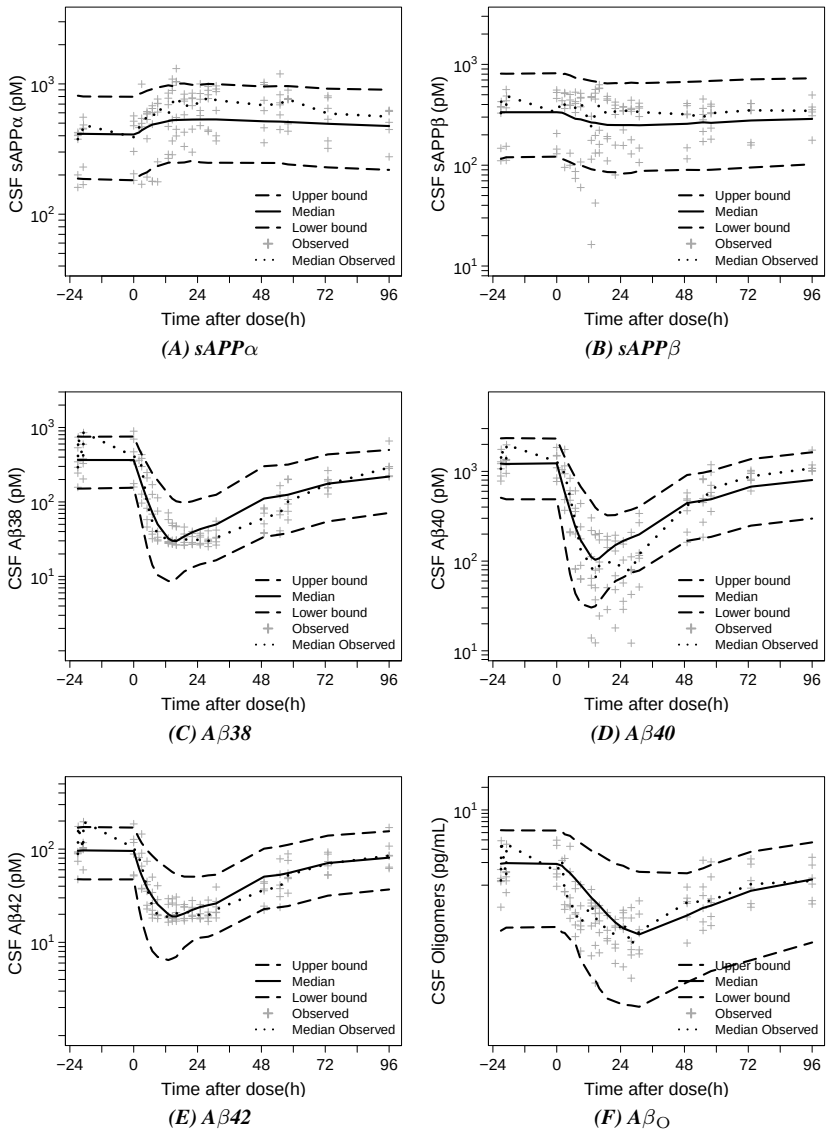

Figure 7.5: Dose 240 mg/kg MK-0752. Visual predictive check of biomarker response* vs. *time profile of MK-0752 in the rhesus with 90% confidence interval. Predictions were performed with extended model ((A), (B),(C), (D), (E),(F)). Observation sample size: n=108 for each APP metabolite from 6 monkeys collected over 4 days.

Plus-symbols represent observed measurements. Dotted blue line corresponds to the median observed profile. Solid lines show the median simulated profiles. The long-dashed lines correspond to the 90% prediction intervals obtained from 1000 individual simulated profiles.

β-γ-O-APP model described all biomarker responses

The β-γ-O-APP model simultaneously described APP metabolite and Aβ_O responses to both BACE1 and GS inhibition. In general, the data were adequately captured across biomarkers for both MBi-5 (Figs. 7.2, 7.3, 7.4) and MK-0752 (Fig. 7.5) treatment. The description of the Aβ responses after MBi-5 treatment was marginally improved compared to the description obtained with the β-O-APP model[11]. The raise in sAPPα after GS inhibition was slightly underpredicted (Fig. 7.5A).

β-γ-O-APP model predicts APP metabolites interrelations

The β-γ-O-APP model could be used to predict APP metabolites interrelations and responses to BACE1 and GS inhibition and foresee the response of APP and C99 in brain (Fig. 7.6).

APP increases after inhibition of BACE1 (Fig. 7.6A), as result of the blocked BACE1 pathway. APP is then shunted down the α-secretase pathway, resulting in an upsurge of sAPPα product. The sAPPβ level reduces after BACE1 inhibition, as it is a direct product of BACE1 cleavage of APP. The increase in sAPPα and decrease in sAPPβ results in a decline in the ratio of sAPPβ:sAPPα and net rise in the sum of sAPPα and sAPPβ (Fig. 7.6E). The C99 level is predicted to decline after BACE1 inhibition. The loss of C99 after BACE1 inhibition results in reduced Aβ levels.

After GS inhibition APP slightly reduces due to the increased α-secretase processing of APP (Fig. 7.6B). As a result of substrate competition sAPPβ also slightly declines. The accumulation of C99 through GS inhibition stimulates the α-secretase pathway, resulting in an upswing of sAPPα levels and changing the ratio of sAPPβ:sAPPα and net sum of sAPPα and sAPPβ (Fig. 7.6F).

Both BACE1 and GS inhibition lower the monomeric Aβ concentrations (Fig. 7.6C, 7.6D), though the respective inhibition results in different Aβ ratios (Fig. 7.6E, 7.6F). Both BACE1 and GS inhibition reduce the Aβ_O level, although the effect is more prolonged after GS inhibition.

The diurnal oscillations observed in the simulated biomarker responses after GS inhibition are induced by the enterohepatic recirculation which MK-0752 exhibits[12,17].

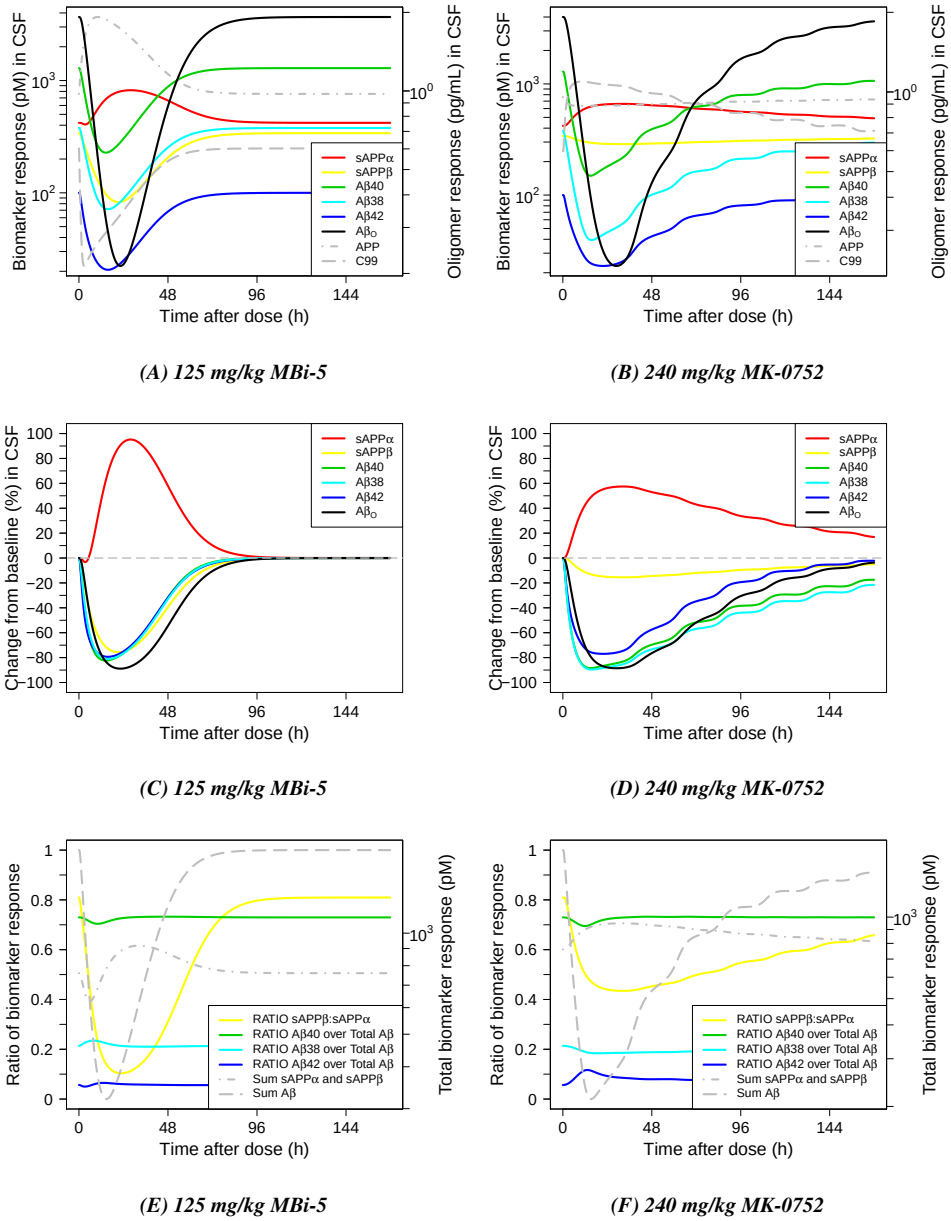

Figure 7.6: Simulation absolute biomarker responses ((A), (B)), biomarker change from baseline (%) ((C), (D)) and biomarker ratios ((E), (F)) using the β-γ-O-APP model. The biomarker responses were simulated after a single dose of 125 mg/kg MBi-5 *(left)* and 240 mg/kg MK-0752 *(right)*, using the typical parameter estimates.
sAPPα red solid line; *sAPPβ* yellow solid line; *Aβ40* green solid line; *Aβ38* light blue solid line; *Aβ42* dark blue solid line; *Aβ_O* black solid line; *C99* grey dot-dashed line; *APP* grey dashed line.

Discussion

One of the main therapeutic strategies is to delay AD onset and progression is reducing Aβ aggregation through the decrease of Aβ monomeric levels by means of Aβ production inhibition. Therefore, the dynamics of Aβ_{O} after Aβ production inhibition needs to be elucidated. The β-γ-O-APP model described APP metabolites (sAPPβ, sAPPα, Aβ38, Aβ40, Aβ42) and Aβ_{O} responses and their interrelations after GS and BACE1 inhibition successfully.

The reduction of Aβ_{O} concentration after inhibition of BACE1 with 125 mg/kg MBi-5 was equivalent to the Aβ_{O} decline obtained after 240 mg/kg MK-0752. The pharmacological effect of GS inhibition was prolonged by the enterohepatic recirculation of MK-0752. The enterohepatic recirculation of MK-0752 was previously discussed by Shou et al. [17].

The simultaneous analysis of BACE1 and GS inhibitor Aβ response data revealed a shift in the relative formation of Aβ38, Aβ40 and Aβ42 after GS blockage. This was explained by stepwise successive cleavage of C99 by GS, in which part of Aβ38 is converted from Aβ42. This pathway is blocked after GS, but not after BACE1 inhibition. Matsumura et al. [20] reported that most of Aβ38 is converted from Aβ42 and Aβ43. Our results indicate that almost a third of Aβ38 originates from Aβ42 cleavage.

sAPPβ and sAPPα are upstream in the APP pathway of the GS cleavage path. To our surprise, sAPPα increased in response to GS inhibition. This could be characterized by a homeostatic feedback loop regulated by C99, where an increase in C99 via GS inhibition stimulates α-secretase processing of APP. This suggests that an increase of membrane bound C99 may affect cellular control of APP α-secretase cleavage or alter APP trafficking to the cell surface, directly or through α-secretase, therefore increasing α-secretase cleavage at the plasma membrane. Enhanced processing of APP by α-secretase after GS inhibition has also been observed in *in vitro* experiments performed in model cell lines reported by Siegenthaler et al. [21]. They suggested that GS activity could influence α-secretase levels or activity. However, the regulation of the activity of α-secretase is not fully understood [6,22].

The observed increase in sAPPα generation was accompanied by a modest reduction of sAPPβ after GS inhibition. This is due to less full-length APP remaining as substrate for BACE1 when α-secretase cleavage is raised. The idea of substrate competition for APP between α-secretase and BACE1 is well accepted [6]. However, here the decrease in sAPPβ is not as strong as would be expected purely based on substrate competition

following the upsurge of α-secretase activity. That is why the model underpredicted the raise in sAPPα. There appears to be an increase in the sum of sAPPβ and sAPPα after GS inhibition (see Supplemental Material, Figure S7.2A). This suggests an increase in production of APP. There may be an autoregulation mechanism of APP production, induced by GS inhibition, compensating for the loss of sAPPβ as result of α-secretase stimulation. This was investigated during model development, and there were indications that including autoregulation of APP would improve the description of the data. However, with the current data, the process of autoregulation could not be characterized adequately. Further investigation is warranted.

Because α-secretase cleaves APP within the Aβ sequence, pharmacological activation of α-secretase, and thereby reducing Aβ production may be a therapeutic intervention in AD. Further, sAPPα plays a role in neuroprotection and is downregulated in familial and sporadic AD patients[22].

Tian et al.[23] proposed a feedback mechanism initiated by the α-secretase cleavage path, in which Aβ production is lowered by increased C83 which negatively modulate GS activity. sAPPα and C83 are products of the same cleavage step by α-secretase. The model predicted increased C83 concentrations as result of BACE1 and GS inhibition. Therefore, this inhibitory effect on GS through C83 is expected to occur after both BACE1 and GS inhibition. The feedback mechanism as proposed by Tian was investigated in the β-γ-O-APP model, but could not be distinguished from the interaction of the inhibitors on the system as both work to lower Aβ levels.

In a series of investigations we have explored the development of a systems pharmacology model for the APP processing pathway. In the first of these investigations, a systems pharmacology model was developed of the APP processing pathway based on CSF concentrations of APP metabolites (Aβ40, Aβ42, sAPPβ, sAPPα) after exposure to the BACE1 inhibitor MBi-5 in CMP rhesus monkeys [16]. With this so called β-APP model, Aβ_O were predicted to reduce after BACE1 inhibition, which was informed from monomeric Aβ species.

In the second investigation, the systems model was validated using tracer kinetic data (fraction labeled sAPPα, fraction labeled sAPPβ and fraction labeled total Aβ). This β-13C-APP model accounted for the tracer $^{13}_{6}$C-Leucine dynamics throughout the systems model [24]. In the third investigation, separate descriptions to characterize the sequential cleavage steps of APP by BACE1 and GS were included in the systems model. This was based on the simultaneous investigation of APP metabolite response data from dedicated studies for the BACE1 inhibitor MBi-5 (Aβ40, Aβ42, sAPPβ, sAPPα) and

the GS inhibitor MK-0752 (Aβ40, Aβ42), respectively [12]. The investigation with this β-γ-APP model implied a difference in Aβ dynamics after BACE1 versus GS inhibition, which was reflected in a different Aβ40 formation rate constant. Further, the model based prediction of Aβ_{O} suggested a lower oligomerization rate of Aβ42 after GS then after BACE1 inhibition. However, in that investigation, the difference in Aβ dynamics between BACE1 *versus* GS inhibition could not be separated from study differences.

In the fourth investigation the β-APP model was extended to describe the effect of an additional Aβ isoform (Aβ38) and capture Aβ_{O} response measurements. This β-O-APP model, was based on simultaneous analysis of CSF APP metabolites (Aβ38, Aβ40, Aβ42, sAPPβ, sAPPα) and Aβ_{O} concentration measurements after MBi-5 exposure [11]. In this investigation, Aβ oligomerization was characterized to be a second order process. Further, Aβ42 was identified to be the Aβ species that drives the Aβ oligomerization

In the current, and hence fifth investigation, the β-O-APP model was extended to describe the effect of BACE1 and GS inhibition on the APP pathway simultaneously and capture Aβ_{O} response data to both inhibitors. With the current analysis, the β-γ-APP model could advance further, as information on the sAPPβ, sAPPα, Aβ38, and Aβ_{O} response data to GS inhibition could be added. Further, seeing the cross-over study design of the current study using both inhibitors, true differences could be separated from study differences. In the current analysis, no differences in systems parameters after BACE1 versus GS inhibition could be identified, which indicated a correct simultaneous characterization of the inhibitor-system interactions. Also, the Hill coefficients shifted to unity, which is the theoretical value for a simple receptor-target interaction, indicating that the β-γ-O-APP model provided a more accurate representation of the inhibitors interaction with the system.

Conclusions & Perspectives

The current and prior series of investigations illustrate that systems pharmacology modelling is work in progress and that various processes in the biological network have to be considered. With each turning, the APP systems model is progressed and biological insights are gained or questions raised that can get the model to an improved or more advanced state.

Here, the β-γ-O-APP model revealed a feedback mechanism by downstream components on a upstream path: blockage of the GS cleavage path promotes the non-amyloidogenic processing of APP by homeostatic feedback, proposed to be exerted

by C99. In addition, the stepwise successive cleavage of C99 by GS, wherein part of Aβ38 is converted from Aβ42 was characterized by the model. Furthermore, the effects of Aβ production inhibition on Aβ_{O} concentrations were quantified.

A next step in the advancement of the APP systems model could be the extension of the model to include higher order agglomerated species, such as fibrils. It would be of interest to know if Aβ production inhibition can bring down the fibril concentrations as well, which may dissociate to Aβ_{O} to restore the balance between these species.

To further evaluate the proposed feedback mechanism, sAPP (sAPPβ and sAPPα) data following a dose range of the GS inhibitor may be informative. Also, sAPP response measurements after an α-secretase stimulator could provide information on a possible autoregulation mechanism of APP production.

The developed β-γ-O-APP model can be used to perform simulations to investigate other interventions, such as inhibition of Aβ oligomerization or Aβ clearance enhancers.

References

1. Jack, C.R. & Holtzman, D.M. Biomarker modeling of Alzheimer's disease. Neuron. 2013;80(6):1347–1358.
2. Klein, W.L. Synaptotoxic amyloid-β oligomers: a molecular basis for the cause, diagnosis, and treatment of Alzheimer's disease? J Alzheimer's Dis. 2013;33:S49–S65.
3. Sengupta, U., Nilson, A.N., & Kayed, R. The Role of Amyloid-β Oligomers in Toxicity, Propagation, and Immunotherapy. EBioMedicine. 2016;6:42–49.
4. Esler, W.P. & Wolfe, M.S. A portrait of Alzheimer secretases - New features and familiar faces. Science. 2001;293(5534): 1449–54.
5. Wiltfang, J., *et al.* Higly conserved and disease-specific patterns of carboxyterminally truncated Aβ peptides 1-37/38/39 in addition to 1-40/42 in Alzheimer's disease and in patients with chronic neuroinflammation. J Neurochem. 2002;81(3):481–496.
6. Lichtenthaler, S.F. Alpha-secretase in Alzheimer's disease: Molecular identity, regulation and therapeutic potential. J Neurochem. 2011;116(1):10–21.
7. Grüning, C.S.R., *et al.* The off-rate of monomers dissociating from amyloid-β protofibrils. J Biol Chem. 2013;288(52): 37104–11.
8. Schmit, J.D., Ghosh, K., & Dill, K. What Drives Amyloid Molecules To Assemble into Oligomers and Fibrils? Biophys J. 2011;100(2):450–458.
9. Cerasoli, E., Ryadnov, M.G., & Austen, B.M. The elusive nature and diagnostics of misfolded Aβ oligomers. Front Chem. 2015;3:17.
10. Takahashi, R.H., Nagao, T., & Gouras, G.K. Plaque formation and the intraneuronal accumulation of β-amyloid in Alzheimer's disease. Pathol Int. 2017;67(4):185–193.
11. van Maanen, E.M., *et al.* Systems pharmacology analysis of the Aβ oligomer response following β-secretase inhibition: Evidence for second-order kinetics of Aβ42 oligomerization. Prep. 2017.
12. van Maanen, E.M., *et al.* Extending a systems model of the APP pathway: Separation of β- and γ-secretase sequential cleavage steps of APP. Submitted. 2017.
13. Gilberto, D.B., *et al.* An alternative method of chronic cerebrospinal fluid collection via the cisterna magna in conscious rhesus monkeys. Contemp Top Lab Anim Sci. 2003;42 (4):53–59.
14. Savage, M.J., *et al.* A sensitive Aβ oligomer assay discriminates Alzheimer's and aged control cerebrospinal fluid. J Neurosci. 2014;34(8):2884–97.
15. Bauer, R.J. 2011 NONMEM users guide. Introduction to NONMEM 7.2.0 Technical report;ICON Development Solutions, Ellicott City, MD.
16. van Maanen, E.M.T., *et al.* Systems pharmacology analysis of the amyloid cascade after β-secretase inhibition enables the identifica-

tion of an Aβ42 oligomer pool. J Pharmacol Exp Ther. 2016;357(1):205–16.

17. Shou, M., *et al.* Population pharmacokinetic modeling for enterohepatic recirculation in Rhesus monkey. Eur J Pharm Sci. 2005;26 (2):151–61.

18. Dobrowolska, J.A., *et al.* Diurnal patterns of soluble amyloid precursor protein metabolites in the human central nervous system. PLoS One. 2014;9(3):e89998.

19. Cook, J.J., *et al.* Acute γ-secretase inhibition of nonhuman primate CNS shifts amyloid precursor protein (APP) metabolism from amyloid-β production to alternative APP fragments without amyloid-β rebound. J Neurosci. 2010;30(19):6743–50.

20. Matsumura, N., *et al.* γ-Secretase associated with lipid rafts: multiple interactive pathways in the stepwise processing of β-carboxyl-terminal fragment. J Biol Chem. 2014;289(8):5109–21.

21. Siegenthaler, B., Bali, J., & Rajendran, L. γ-Secretase regulates the α-secretase cleavage of the Alzheimer's disease, amyloid precursor protein. Matters. 2016;pages 1–7.

22. Vingtdeux, V. & Marambaud, P. Identification and biology of α-secretase. J Neurochem. 2012;120 (Suppl. 1):34–45.

23. Tian, Y., Crump, C.J., & Li, Y.M. Dual Role of α-Secretase Cleavage in the Regulation of γ-Secretase Activity for Amyloid Production. J Biol Chem. 2010;285(42): 32549–32556.

24. Van Maanen, E.M., *et al.* Integrating tracer kinetic data into a systems pharmacology model of the amyloid precursor pathway - effect of a β-secretase inhibitor. Prep. 2017.

Chapter 7

Supplemental Material

Supplement to

A single systems pharmacology approach to unravel Aβ oligomer modulation upon administration of multiple APP cleavage inhibitors

E.M.T. van Maanen, T.J. van Steeg, J. Kalinina, M.S. Michener, M.J. Savage, M.E. Kennedy, J.A. Stone, M. Danhof

SUPPLEMENTAL MATERIAL

Differences in Aβ ratios after BACE1 *versus* GS inhibition

The sum of Aβ38, Aβ40 and Aβ40 in the treatment arms of the cross-over study is presented in Fig. S7.1A. Both BACE1 and GS inhibition resulted in a reduction of total Aβ. The ratios of Aβ38, Aβ40 and Aβ40 over total Aβ is depicted in Fig. S7.1B. GS inhibition resulted in a bigger change in the ratios of each Aβ species over total, compared to BACE1 inhibition, with the investigated dosages. The difference is most pronounced for the ratio Aβ42 over total Aβ.

Differences in the sum and ratio of sAPPβ and sAPPα after BACE1 *versus* GS inhibition

The sum of sAPPβ and sAPPα and the ratio of sAPPβ over sAPPα in the treatment arms of the cross-over study is depicted in Fig. S7.2A and S7.2B, respectively. Both BACE1 and GS inhibition reduce the ratio of sAPPβ over sAPPα.

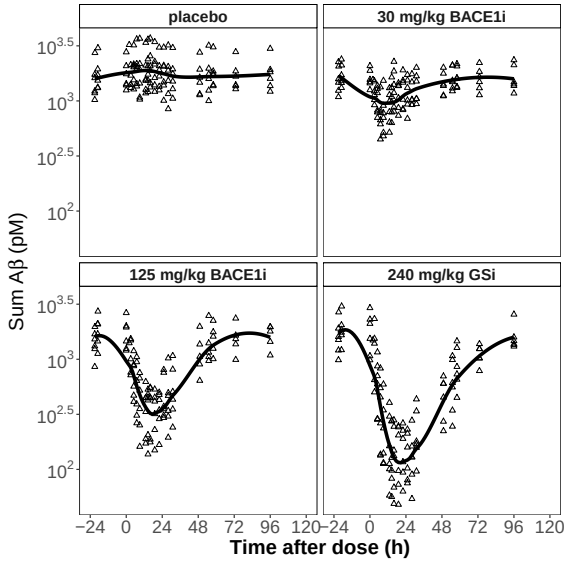

(A) Sum of Aβ

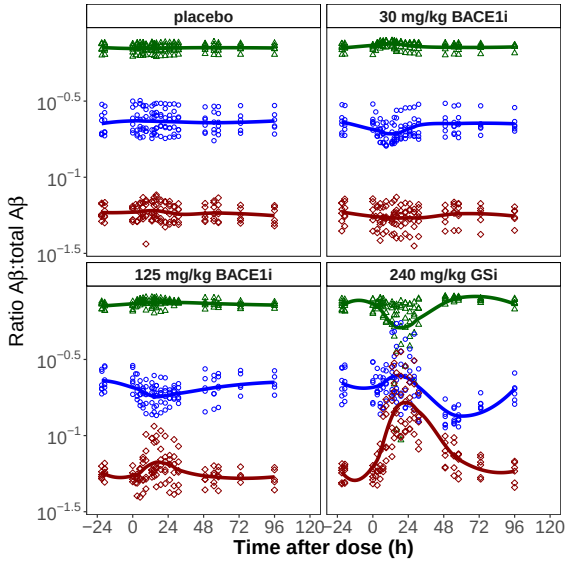

(B) Ratio of Aβ

Figure S7.1: Observed differences in the treatment arms of the sum of Aβ38, Aβ40 and Aβ42 (A) and the ratio of each Aβ species over total Aβ (B). The lines are smoothers through the observed data.
Black: sum of Aβ; *Green*: ratio Aβ40 over total Aβ; *Blue:* ratio Aβ38 over total Aβ; *Red:* ratio Aβ42 over total Aβ.

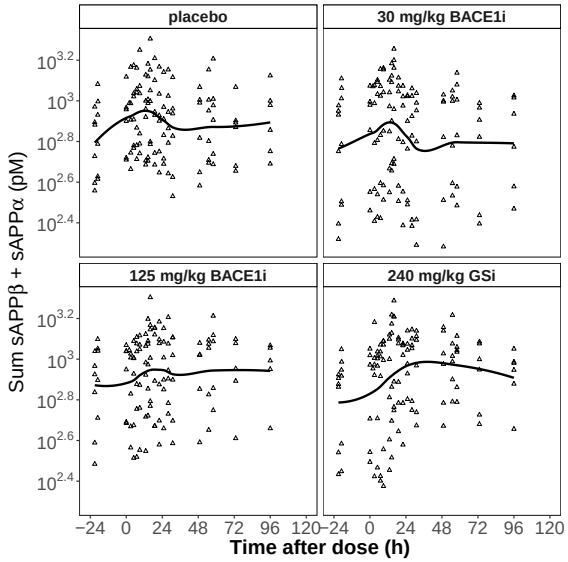

(A) Sum of sAPPβ and sAPPα

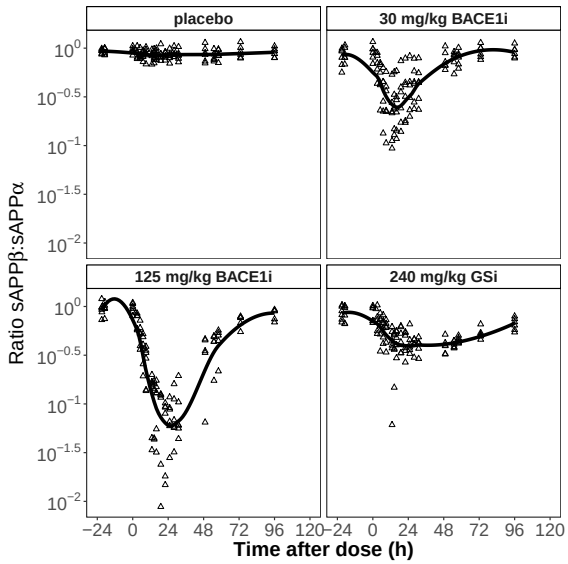

(B) Ratio sAPPβ:sAPPα

Figure S7.2: Observed differences in the treatment arms of the sum of sAPPα and sAPPβ (A) and the ratio of sAPPβ over sAPPα (B). The lines are smoothers through the observed data.